Localization of Floquet states along a continuous line of periodic orbits

T. Timberlake and F. Petruzielo
Department of Physics, Astronomy, and Geology, Berry College, Mount Berry, Georgia 30149-5004, USA

L. E. Reichl
Center for Studies in Statistical Mechanics and Complex Systems, The University of Texas at Austin, Austin, Texas 78712, USA
(Received 18 March 2005; published 15 July 2005)

A periodically driven particle in an infinite square well is shown to exhibit quantum localization due to a continuous line of periodic orbits in the classical system. Individual Floquet eigenstates localized along this line of periodic orbits are identified. The enhanced localization persists for field strengths beyond that at which the continuous line of orbits is destroyed in the classical dynamics. These results may be relevant to experiments involving trapping potentials with flat regions.

DOI: 10.1103/PhysRevE.72.016208 PACS number(s): 05.45.Mt, 73.20.Jc, 73.20.Fz

I. INTRODUCTION

Studies of the quantum dynamics of systems whose classical counterpart is chaotic have led to a number of surprising results [1]. One such result is the localization of some quantum eigenstates in chaotic regions of the underlying classical phase space. The localization of eigenstates is due to several different mechanisms. Some localized quantum eigenstates, called scars, have probability densities peaked along isolated unstable periodic orbits of the classical motion. Scarred eigenstates have been observed in a variety of physical systems [2]. Localized eigenstates also occur in disordered systems due to dynamic Anderson localization [3] and in regions of phase space containing cantori [4].

Another source of localized states is *nonisolated*, marginally stable (parabolic) periodic orbits of the classical motion. The "bouncing ball" (BB) states of the stadium billiard fall into this category [5]. These BB states have been observed in a variety of billiard systems [6], and their effects have been measured experimentally [7]. "Bouncing ball" states survive in the classical limit ($E\to\infty$ or $\hbar\to 0$). However, since the BB states form a set of measure zero in this limit, they conform to the theorems of Schnirelman, Zelditch, and Colin de Verdiere [8] which indicate that in the classical limit all but a set of measure zero of the quantum eigenstates must conform to the domain of typical classical trajectories.

In the sections below, we show that a continuous line of marginally stable periodic orbits can be created in systems that are continuously driven by a periodic force and that these orbits give rise to localized Floquet eigenstates of the driven system. These orbits can exist in regions of the phase space where the unperturbed potential is flat. We study this effect by analyzing a sinusoidally driven particle in an infinite square well. In Sec. II A, we review the classical dynamics of our model and show the existence of a continuous line of marginally stable periodic orbits that never collide with the walls of the well. After a brief overview of the quantum dynamics of time-periodic systems in Sec. II B, we show in Sec. III that the quantum dynamics of our model exhibits localization along the line of orbits and that this region of enhanced localization changes to correspond with changes in the line of orbits as the strength of the driving field is increased. In Sec. IV, we identify individual Floquet eigenstates that are localized along the line of orbits (which we dub "zero-collision" states) and show that their localization is greater than would be predicted based on random matrix theory (RMT) and symmetry considerations. In Sec. V, we show that the enhanced localization and zero-collision states remain for field strengths beyond that at which the line of orbits disappears, even though the classical motion is highly chaotic for these field strengths.

II. DYNAMICAL MODEL

The model we use to study the effect of flat regions of the confining potential is a periodically driven particle in a one-dimensional infinite square well. The Hamiltonian for this system is

$$\tilde{H}(t)=\frac{\tilde{p}^2}{2m}+V_{SQ}(\tilde{x})+\tilde{\epsilon}\tilde{x}\cos(\tilde{\omega}_0\tilde{t}), \tag{1}$$

where $\tilde{p}$ and $\tilde{x}$ are the momentum and postion, respectively, of the particle. The square-well potential $V_{SQ}(\tilde{x})$ has a width $2a$ such that $V_{SQ}(\tilde{x})=0$ for $|\tilde{x}|\leqslant a$ and $V_{SQ}(\tilde{x})=\infty$ for $|\tilde{x}|>a$. The strength of the dipole coupling between the particle and radiation field is $\tilde{\epsilon}$, the frequency of the field is $\tilde{\omega}_0$, and the time is $\tilde{t}$. We can write this Hamiltonian in terms of dimensionless parameters with the following scaling transformation [9]: $\tilde{H}=Hc$, $\tilde{x}=xa$, $\tilde{p}=p\sqrt{2mc}$, $\tilde{\epsilon}=\epsilon c/a$, $\tilde{t}=ta\sqrt{2m/c}$, and $\tilde{\omega}_0=\omega_0\sqrt{c/(2ma^2)}$. In terms of dimensionless variables, the Hamiltonian then takes the form

$$H(t)=p^2+V_{SQ}(x)+\epsilon x\cos(\omega_0 t), \tag{2}$$

where the scaled square-well potential $V_{SQ}(x)$ now has the form $V_{SQ}(x)=0$ for $|x|\leqslant 1$ and $V_{SQ}(x)=\infty$ for $|x|>1$. This transformation introduces an arbitrary unit of energy c. The transformation $(\omega_0,\epsilon)\to(\omega_0\sqrt{c},\epsilon c)$ leaves the dynamics unchanged except for a scaling of the energy by a factor of c, so only one of these two parameters is independent. We can obtain a complete picture of the dynamics of the system by choosing an arbitrary value for ω_0 (in this paper $\omega_0=80$) and investigating the dynamics as ϵ is varied. The Hamiltonian is

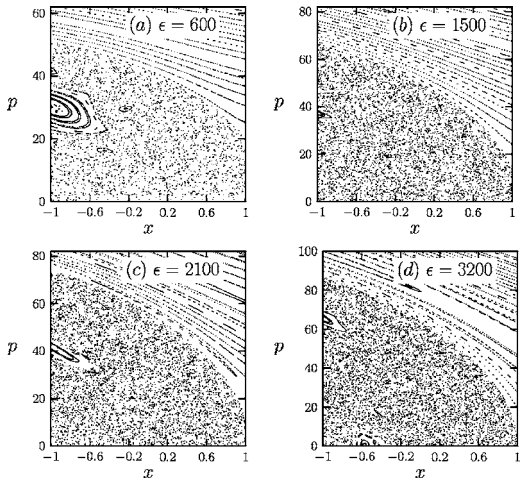

FIG. 1. Strobe plots of the classical dynamics at various field strengths. In (a) the $l=1$ primary resonance is visible at the left wall near $p=30$. The chaotic region remains confined to low momenta at all field strengths, but grows in size as ϵ is increased. A continuous line of periodic orbits runs along $p=0$ from $x=4\epsilon/\omega_0^2-1$ to $x=1$ (this line of orbits is not visible in the strobe plots). Note that only the $p\geqslant 0$ portion of the phase space is shown because the system is symmetric in p.

invariant under the transformation $p\rightarrow -p$ and under a generalized parity transformation defined by $x\rightarrow -x$, $t\rightarrow t+T/2$. For $\epsilon=0$, of course, the Hamiltonian is invariant under the more conventional parity transformation $x\rightarrow -x$.

A. Classical system

For the classical system, we can rewrite the Hamiltonian in terms of action-angle variables (J,θ) if we introduce the canonical transformation $J=2|p|/\pi$ and $\theta=\pi\,\mathrm{sgn}(p)(x+1)/2$. The Hamiltonian then takes the form

$$H(t)=\frac{\pi^2 J^2}{4}-\frac{4\epsilon}{\pi^2}\sum_{\substack{l=-\infty\\ l\ \mathrm{odd}}}^{\infty}\frac{1}{l^2}\cos(l\theta-\omega_0 t). \tag{3}$$

Nonlinear resonances occur at values of the action given by $J_l=2\omega_0/(l\pi^2)$ or momenta given by $|p_l|=\omega_0/(l\pi)$ where l is an odd integer that labels the resonances. The higher-order resonances are at low momenta, and the resonances become more closely spaced as l increases. As ϵ is increased these resonances grow and overlap, forming a region of chaotic motion in the low-momentum part of phase space. Figure 1 shows strobe plots of the classical dynamics for this system at several field strengths. The $l=1$ resonance is visible as a series of nested elliptical curves near $p=30$ for $\epsilon=600$ [Fig. 1(a)], but already at this field strength this resonance island is surrounded by a sea of chaotic motion. Trajectories at high values of momentum remain regular. As ϵ is increased [Figs. 1(b)–1(d)] the chaotic sea grows toward higher momentum and the regular structures within the chaotic region disappear or diminish in size. Note, however, the appearance of a new regular island near $p=0$ and $x=-0.6$ for $\epsilon=3200$ [Fig. 1(d)].

One regular structure which is not visible in the strobe plots is a line of marginally stable periodic orbits that lie along $p=0$. This line occupies zero area in phase space, so we do not expect it to be visible in the strobe plots. However, the existence of this line of periodic orbits is easy to show. Let us for the moment ignore the walls of the square well and consider the motion of a free particle in the periodic driving field. The Hamiltonian equations of motion for this system can be easily solved to find

$$x(t)=x_0+p_0 t+\frac{2\epsilon}{\omega_0^2}[\cos(\omega_0 t)-1], \tag{4}$$

$$p(t)=p_0-\frac{2\epsilon}{\omega_0}\sin(\omega_0 t), \tag{5}$$

where x_0 and p_0 are the initial values of position and momentum, respectively. If we now bring back the walls of our square well, we see that there is a family of trajectories that never hit either of the walls. Specifically, trajectories with $p_0=0$ and $4\epsilon/\omega_0^2-1<x_0<1$ will oscillate between the walls of the well without colliding with either wall. We will refer to these orbits as zero-collision (ZC) orbits. These trajectories are only marginally stable. Making p_0 nonzero results in a trajectory that drifts slowly toward one wall or the other as it oscillates, so that the trajectory will eventually collide with one of the walls and diffuse throughout the chaotic region of phase space. Also note that the condition on x_0 for the ZC orbits can only be satisfied if $\epsilon<\omega_0^2/2$. So for $\omega_0=80$ the line of ZC orbits will not exist for $\epsilon>3200$.

B. Quantum system

To analyze the quantum dynamics of our model we calculate the Floquet eigenstates of the system [10]. The Floquet Hamiltonian is given by $H_F(t)\equiv H(t)-i\partial/\partial t$ and has eigenstates obtained by solving the eigenvalue equation

$$H_F(t)|\phi_\alpha(t)\rangle=\Omega_\alpha|\phi_\alpha(t)\rangle, \tag{6}$$

where $|\phi_\alpha(t)\rangle$ is the αth Floquet eigenstate and Ω_α is the αth Floquet eigenvalue. Here we have set the value of the dimensionless scaled Planck's constant $[\hbar_s=\hbar/(a\sqrt{2mc})]$ to 1. The Floquet eigenstates have period $T_0=2\pi/\omega_0$, so $|\phi_\alpha(t+T_0)\rangle=|\phi_\alpha(t)\rangle$. These eigenstates form a complete orthonormal basis which determines the dynamics. The Floquet eigenphases, Ω_α, are conserved quantities [1,11].

When the system is in an arbitrary quantum state $|\psi(0)\rangle$ at time $t=0$, the state of the system at time t can be written

$$|\psi(t)\rangle=\sum_\alpha\langle\phi_\alpha(0)|\psi(0)\rangle e^{-i\Omega_\alpha t}|\phi_\alpha(t)\rangle. \tag{7}$$

The Floquet evolution operator $\hat{U}_F(T_0)$ can be defined as

$$\hat{U}_F(T_0)=\sum_\alpha e^{-i\Omega_\alpha T_0}|\phi_\alpha(0)\rangle\langle\phi_\alpha(0)|, \tag{8}$$

and the state of the system at time $t=T_0$ takes on an especially simple form $|\psi(T_0)\rangle=\hat{U}_F(T_0)|\psi(0)\rangle$.

We can compute matrix elements of the Floquet evolution operator in the basis of unperturbed energy eigenstates $|E_n\rangle$ of the square-well potential. The (n,n')th matrix element of

the resulting Floquet matrix is given by $U_{n,n'}(T_0) = \langle E_n | \hat{U}_F(T_0) | E_{n'} \rangle$. The αth eigenvalue of the Floquet matrix $U_{n,n'}(T_0)$ is $\exp(-i\Omega_\alpha T_0)$, and the αth eigenvector in the unperturbed energy basis is given by a column matrix composed of matrix elements $\langle E_n | \phi_\alpha(0) \rangle$, where $n=1,\ldots,\infty$. The eigenvalues Ω_α can be obtained from $\exp(-i\Omega_\alpha T_0)$, but only modulo ω_0.

Due to the symmetries of the Hamiltonian, the Floquet states of our model can be classified as even or odd under the generalized parity transformation and they will have probability distributions that are symmetric about the line $p=0$.

We numerically calculate the matrix $U_{n,n'}(T_0)$ using a basis consisting of the first 120 energy eigenstates $|E_n\rangle$ of the infinite square well. This basis extends well into the regular region of the phase space and should therefore be sufficient to accurately calculate all of the quantum eigenstates associated with the chaotic region. The eigenstates of the Floquet operator can be determined numerically [12] and will be of the form

$$|\phi_\alpha\rangle = \sum_n c_{\alpha,n} |E_n\rangle. \tag{9}$$

We can examine the distribution of probablity in phase space for each Floquet eigenstate by constructing a Husimi distribution for the eigenstate [13]. The Husimi distribution is a quasiprobability distribution (smoothed on the scale of $\hbar_s$) for the Floquet state in phase space. To construct the Husimi distribution we must first calculate the overlap of each eigenstate with a Gaussian wave packet centered at the point (x_0,p_0). The wave function for the Gaussian wave packet in dimensionless units is

$$\langle x | x_0,p_0 \rangle = \frac{1}{(\sigma^2\pi)^{1/4}} \exp\left(-\frac{(x-x_0)^2}{2\sigma^2} + ip_0(x-x_0) \right). \tag{10}$$

The width of this Gaussian wave packet is $\Delta x = \sigma/\sqrt{2}$ in the x direction and $\Delta p = 1/(\sigma\sqrt{2})$ in the p direction. In this paper we use $\sigma = 0.0892$. The Husimi distribution for the Floquet eigenstate $|\phi_\alpha\rangle$ is constructed by calculating $h_\alpha(x_0,p_0) = |\langle x_0,p_0 | \phi_\alpha \rangle|^2$ on a grid of points in phase space.

III. LOCAL INVERSE PARTICIPATION RATIO

To identify regions of phase space in which the quantum system shows enhanced localization we calculate the local inverse participation ratio (LIPR) $\mathcal{L}(x_0,p_0)$, which is the mean-squared Floquet-state intensity at the point (x_0,p_0) averaged over all of the Floquet states [14]:

$$\mathcal{L}(x_0,p_0) = \frac{\frac{1}{N}\sum_{\alpha=1}^{N} [h_\alpha(x_0,p_0)]^2}{\left(\frac{1}{N}\sum_{\alpha=1}^{N} h_\alpha(x_0,p_0) \right)^2}, \tag{11}$$

where $N=120$ is the number of Floquet eigenstates. Higher values of $\mathcal{L}(x_0,p_0)$ indicate a greater degree of localization

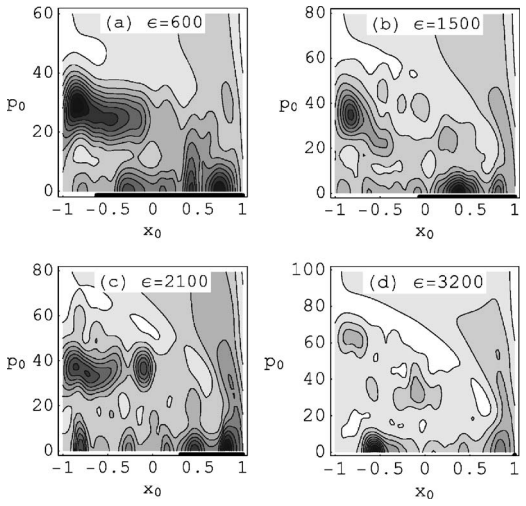

FIG. 2. Local inverse participation ratio $\mathcal{L}(x_0,p_0)$ as a function of phase-space location for several field strengths. Dark regions indicate high values of $\mathcal{L}(x_0,p_0)$ and therefore areas of increased localization. The thick, solid line at the bottom of each plot indicates the range of x values covered by the line of periodic orbits that runs along $p=0$. Note that $\mathcal{L}(x_0,p_0)$ is peaked along the line of periodic orbits in (a), (b), and (c). In (d) the line of orbits has shrunk to a single point, but there is still a small increase in $\mathcal{L}(x_0,p_0)$ in that vicinity.

near (x_0,p_0). The LIPR has been shown to be an effective measure of quantum localization in the stadium billiard [14]. If eigenstates in a chaotic region of phase space are assumed to be random superpositions of plane waves, then their overlap with a Gaussian wave packet should follow a χ^2 distribution with two degrees of freedom and the expected value for the LIPR is $\mathcal{L}(x_0,p_0)=2$. However, along symmetry lines (such as $p=0$ in our model) the Gaussian wave packets are real and the overlap with the Floquet states will follow a χ^2 distribution with only one degree of freedom, giving $\mathcal{L}(x_0,p_0=0)=3$ [14]. So we expect to see an enhancement of $\mathcal{L}(x_0,p_0)$ by a factor of 1.5 along $p_0=0$ due to symmetry.

We calculate $\mathcal{L}(x_0,p_0)$ on a 129×129 grid of points in phase space with values of p_0 ranging from -125 to 125. Contour plots of $\mathcal{L}(x_0,p_0)$ for various field strengths are shown in Fig. 2. Note that only the region with $p_0 \geqslant 0$ is shown because $\mathcal{L}(x_0,p_0)$, like $h(x_0,p_0)$, is symmetric about the line $p=0$. In all four parts of Fig. 2, $\mathcal{L}(x_0,p_0)$ has a significant peak in the regions of phase space occupied by the classical nonlinear resonance islands seen in Fig. 1. This is expected since resonance regions are occupied by only a few Floquet states which are localized in those regions. There are also significant peaks in $\mathcal{L}(x_0,p_0)$ along the line $p_0=0$. We find that the value of $\mathcal{L}(x_0,p_0)$ at these peaks is significantly higher than would be expected based on the fact that $p=0$ is a symmetry line. Even if the value of $\mathcal{L}$ at these peaks is reduced by a factor of 1.5 to offset the effects of symmetry, the values are still more than two standard deviations greater than the mean.

Perhaps the strongest evidence that the enhancement of $\mathcal{L}(x_0,p_0)$ along $p_0=0$ is not due solely to symmetry effects is that the peaks in $\mathcal{L}(x_0,p_0)$ change their location in phase

space as ϵ is increased. The enhancement of $\mathcal{L}(x_0,p_0)$ due to symmetry should occur uniformly along the line $p_0=0$. Instead, Fig. 2 shows a nonuniform distribution with well-defined peaks. For comparison, we show at the bottom of each plot in Fig. 2 a line indicating the values of x_0 covered by the line of periodic orbits discussed in the previous section. Note that as ϵ is increased the most prominent peaks in $\mathcal{L}(x_0,p_0)$, outside of the resonance regions, lie along the line of periodic orbits. For $\epsilon=3200$ there is a very prominent peak near $x_0=-0.6$ but inspection of Fig. 1(d) shows that this is the location of a classical resonance island at this field strength. Based on this observed behavior we conclude that the strong peaks in $\mathcal{L}(x_0,p_0)$ in the vicinity of the line of periodic orbits are not due to symmetry effects, but rather represent a genuine enhancement of quantum localization as a result of the line of periodic orbits. We also note that a few other minor peaks in $\mathcal{L}(x_0,p_0)$ occur within the chaotic region of phase space at all of the field strengths shown. These peaks may be due to scarring on unstable periodic orbits.

IV. INVERSE PARTICIPATION RATIO OF FLOQUET EIGENSTATES

To provide additional evidence linking quantum localization to the line of periodic orbits we compute the inverse participation ratio (IPR) of each Floquet state. The inverse participation ratio $\mathcal{I}_\alpha$ for the αth Floquet eigenstate is

$$\mathcal{I}_\alpha = \frac{\frac{1}{J}\sum_{j=1}^{J}[h_\alpha(x_j,p_j)]^2}{\left(\frac{1}{J}\sum_{j=1}^{J}h_\alpha(x_j,p_j)\right)^2}, \tag{12}$$

where j is an index labeling the phase-space points in the grid used to calculate the Husimi distribution and J is the number of those grid points. The IPR has been shown to be an effective measure of the localization of an individual eigenstate [14] (larger values of $\mathcal{I}_\alpha$ imply greater localization). Some highly localized states lie in the high-momentum regular region of phase space, and to distinguish between these states and localized states that lie in the low-momentum chaotic region, we plot $\mathcal{I}_\alpha$ versus the energy expectation value ($H_\alpha=\langle\phi_\alpha|p^2|\phi_\alpha\rangle$) of each Floquet state. The results, for several field strengths, are shown in Fig. 3.

Figure 3(a) shows the plot of $\mathcal{I}_\alpha$ versus H_α for $\epsilon=600$. For large values of H_α there is a regular sequence of points with roughly constant $\mathcal{I}_\alpha$ which correspond to Floquet states that lie in the high-energy regular region of phase space. There is also a sequence of points (indicated by solid squares) with $H_\alpha\approx 800$ and a range of values for $\mathcal{I}_\alpha$. These points correspond to Floquet states that lie within the region of phase space occupied by the $l=1$ resonance island seen in Fig. 1(a). The remainder of the points correspond to Floquet states that lie within the chaotic region of Fig. 1(a). Four of these states (indicated by solid triangles) have much higher values of $\mathcal{I}_\alpha$ than do the rest of the chaotic states. Husimi distributions for these four states are shown in Fig. 4. It is clear that all four of these states are peaked along the line of periodic orbits

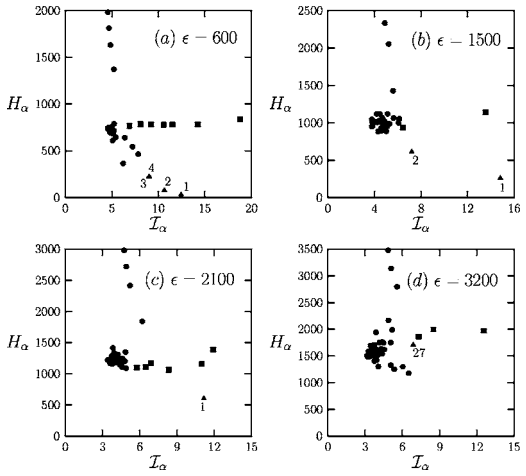

FIG. 3. Plots of $\mathcal{I}_\alpha$ versus H_α for several field strengths. At high values of H_α the points form a regular sequence. These points correspond to states located in the high-momentum regular region of phase space. Points indicated by solid squares correspond to states that lie in or around a resonance island. Points indicated by solid triangles (and labled by a state number α) correspond to Floquet states that are peaked along the line of orbits. Husimi distributions for these states are shown in Figs. 4 and 5. Note that for each field strength the states peaked on the line of orbits have the highest values of $\mathcal{I}_\alpha$ of any state that does not lie in or near a resonance island.

(which is indicated by the thick line at the bottom of each plot). We designate such states as ZC states since they are peaked along the line of classical orbits that never collide with either wall.

Figures 3(b)–3(d) show plots of $\mathcal{I}_\alpha$ versus H_α for higher field strengths. In each case Floquet states that lie within a classical resonance region are indicated with solid squares and ZC states are indicated with solid triangles. Husimi dis-

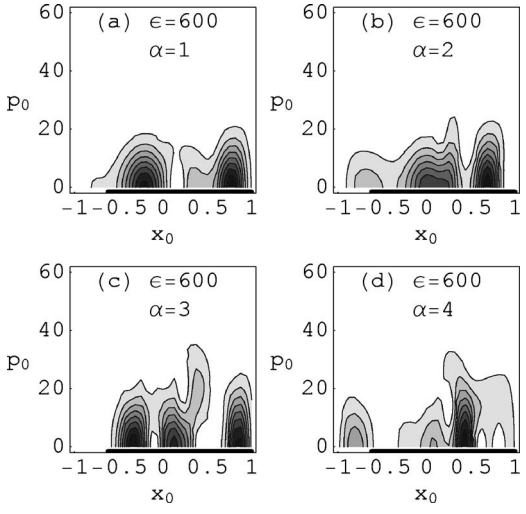

FIG. 4. Husimi distributions of the first four Floquet eigenstates (ordered by increasing value of $\langle p^2\rangle$) for $\epsilon=600$. The thick, solid line at the bottom of each plot indicates the range of x_0 values covered by the line of periodic orbits that runs along $p_0=0$. Note that all four states are peaked along the line of periodic orbits.

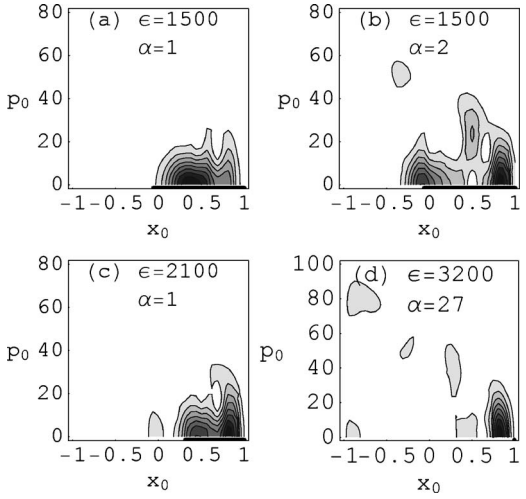

FIG. 5. Husimi distributions of Floquet eigenstates that are peaked along the line of periodic orbits for several field strengths. The thick, solid line at the bottom of each plot indicates the range of x_0 values covered by the line of periodic orbits that runs along $p_0=0$. The index α labels the Floquet state by increasing value of $\langle p^2 \rangle$ for each field strength.

tributions of these ZC states are shown in Fig. 5. Note that for each field strength the ZC states have the highest $\mathcal{I}_\alpha$ values of all of the low-energy chaotic states (not including the resonance island states). The Husimi distributions of all of the low-energy Floquet states were examined for many field strengths and in each case we found that the highest IPR values for states lying in the chaotic region of phase space were those of the ZC states.

In the stadium billiard, some localized quantum states exist because of the large energy separation between adiabatic basis states at low energies while others (the BB states) exist because of the presence of families of marginally stable periodic orbits [15]. It is important to point out that, although the Husimi distributions for the ZC states at $t=0$ resemble that of the ground state of the infinite square well, the ZC states are not a low-energy phenomenon. The Husimi distributions shown in Figs. 4 and 5 show the ZC states at one phase of the driving field and thus do not provide a complete picture of the average energy of these states over one cycle of the field. To see that this effect is not confined to low energies note that the average energy of a classical ZC orbit over one cycle of the field is $2\epsilon^2/\omega_0^2$. This quantity is quite large for many of the field strengths we have examined in this paper.

Another concern is that the increased values of $\mathcal{I}_\alpha$ for the ZC states might be due to the symmetry effects described in Sec. III. Random matrix theory predicts a Porter-Thomas distribution of wave function intensities in the chaotic region of phase space, leading to $\mathcal{I}_\alpha=2$ for complex wave functions [14]. Our Floquet eigenstates are real, but the Gaussian wave packets used to calculate the Husimi distribution are in general complex. Along the line $p_0=0$, however, the Gaussian wave packets are real which leads to a RMT value of $\mathcal{I}_\alpha=3$. The line of symmetry artificially enhances $\mathcal{I}_\alpha$ by a factor of 1.5. To determine if this symmetry effect is solely responsible for the enhanced IPR values of the ZC states, we identified (by visual inspection of the Husimi distrubitons) the state most strongly peaked on the line of orbits at each field strength and found the value of $\mathcal{I}_\alpha$ for this state. We also examined the Husimi distributions to identify which Floquet states lie in the chaotic region of phase space so that we could calculate the mean value of $\mathcal{I}_\alpha$ for this set of states. Figure 6 shows a plot of the IPR of the ZC state versus field strength. For comparison, we also show the mean IPR of all the chaotic states as well as the predicted value of $\mathcal{I}_\alpha$ from RMT.

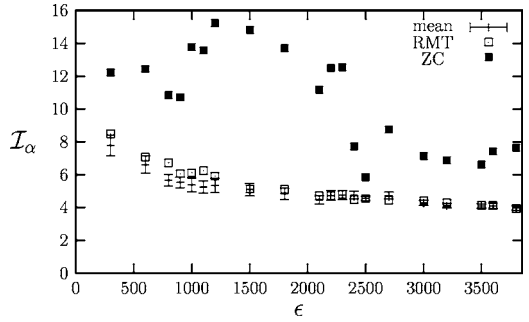

FIG. 6. Plot of the value of $\mathcal{I}_\alpha$ as a function of field strength for the state most closely identified with the line of periodic orbits. For comparison we show the mean $\mathcal{I}_\alpha$ of all chaotic states and the RMT prediction for $\mathcal{I}$. Error bars for the mean $\mathcal{I}_\alpha$ are determined by dividing the standard deviation by the square root of the number of chaotic states.

The RMT values have been scaled to account for the fact that only a part of the region of phase space on which the Husimi distributions were calculated is chaotic. From the definition of the IPR [Eq. (12)] we see that the RMT value for a fully chaotic phase space ($\mathcal{I}_\alpha=2$) must be multiplied by J/K, where J is the total number of grid points used in calculating the Husimi distribution and K is the number of those points that lie within the chaotic region of phase space. We estimate this ratio using the ratio of the area of the chaotic region to the area of the region on which the Husimi distributions are calculated. From Fig. 6 it is clear that the IPR of the ZC state is much higher than the average IPR for all chaotic states or the prediction of RMT for all field strengths. Indeed, even if the IPR of the ZC state is reduced by a factor of 1.5, it still remains much higher than the average for all chaotic states for $1000<\epsilon<2400$. This is a clear indication that the enhancement of the IPR for the ZC states is not due solely to the fact that they lie along a line of symmetry. Note that the average value of $\mathcal{I}_\alpha$ for the chaotic states is in good agreement with the prediction of RMT.

V. DISAPPEARANCE OF THE ZERO-COLLISION ORBITS

The zero-collision states of our model are very similar to the bouncing ball states of the stadium and other billiard systems. However, there is at least one important difference. In the stadium billiard the BB orbits are trajectories that bounce back and forth between the horizontal straight-line segments of the stadium boundary. For each point along this horizontal segment there is a corresponding BB orbit at any energy. Therefore the BB orbits form a one parameter family

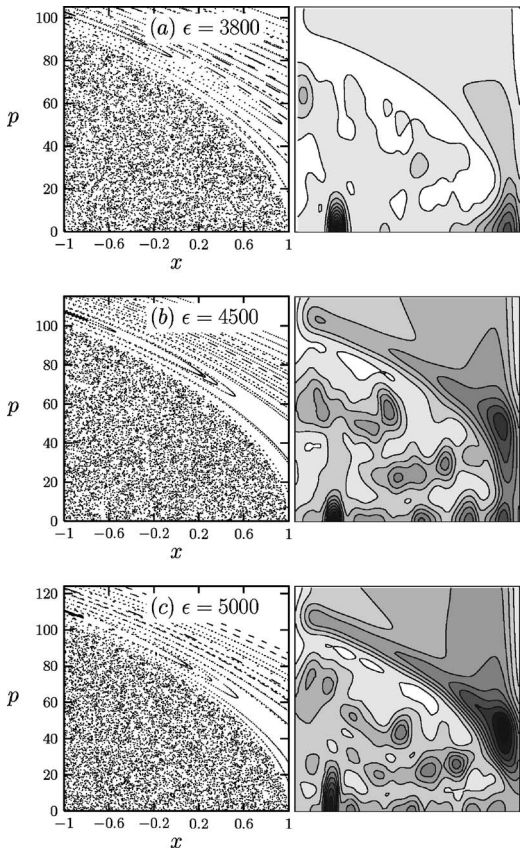

FIG. 7. The plots on the left are strobe plots of the classical motion at three field strengths for which the line of periodic orbits along $p=0$ no longer exists. The plots on the right show $\mathcal{L}(x_0,p_0)$ as a function of phase-space location for the same field strengths, where the horizontal and vertical axes on the right-hand plots, x_0 and p_0, respectively, take the same range of values as x and p on the left-hand plots. Note that at $\epsilon=3800$ there is still a prominent peak in $\mathcal{L}(x_0,p_0)$ near the right wall at $p_0=0$. For $\epsilon=5000$ this peak has moved well away from $p_0=0$.

of periodic orbits for any given energy. To make this family of orbits disappear one must reduce the length of the horizontal segment of the boundary to zero. In this limit the stadium billiard turns into a circular billiard, which is a classically integrable system. In our model, the ZC orbits also form a one-parameter family of periodic orbits. However, our model does not become integrable in the limit in which the family of ZC orbits disappears. No ZC orbits will be found for $\epsilon>3200$ in our model, but for these fields strengths the classical dynamics in the region of phase space around $p=0$ is chaotic. We would like to know what happens to the ZC states when the ZC orbits no longer exist.

Figure 7 shows strobe plots of the classical motion and contour plots of the LIPR (see Sec. III) as a function of phase-space location for $\epsilon=3800$, 4500, and 5000. Note that in Fig. 7(a) ($\epsilon=3800$) there is a significant peak in $\mathcal{L}(x_0,p_0)$ near $(x_0=1,\ p_0=0)$, which is the location of the last ZC orbit at $\epsilon=3200$. In Fig. 7(b) ($\epsilon=4500$) this peak is still visible but there is a more prominent peak near $(x_0=1,\ p_0=40)$ which appears to be the location of an unstable periodic orbit that lies on the separatrix of a newly formed resonance. In Fig. 7(c) there is no visible peak at $(x_0=1,\ p_0=0)$. Instead there is a very prominent peak near the apparent unstable periodic orbit at $(x=1,\ p=40)$. These results indicate that the effects of the ZC orbits do not disappear as soon as the orbits themselves do. Indeed, there seems to be increased localization in the vicinity of the last ZC orbit for values of ϵ well beyond the value at which that last ZC orbit disappears. Investigation of the classical dynamics in that region of phase space shows no sign of any stable classical structures. This increased localization may be an example of scarring by ghosts of periodic orbits, where "ghosts" are defined to be periodic orbits that do not exist in the classical system but rather in some *neighboring* classical system. In our model, a neighboring system would correspond to the same model with a slightly different value for ϵ. Pseudointegrable triangle billiards have been shown to have quantum eigenstates scarred on families of periodic orbits that exist in neighboring billiards (triangles with slightly different angles) [16]. Further work is needed to verify whether or not the enhanced localization in our model near $(x=1,\ p=0)$ for $\epsilon>3200$ is due to this ghost effect.

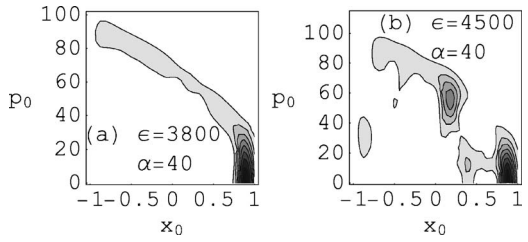

FIG. 8. Husimi distributions of Floquet states that are peaked near $(x_0=1,\ p_0=0)$ for $\epsilon=3800$ and $\epsilon=4500$. For $\epsilon=5000$ we were unable to find a Floquet state that was peaked near $(x_0=1,\ p_0=0)$.

Husimi distributions of low-energy Floquet states were also examined for $\epsilon=3800$, 4500, and 5000. For $\epsilon=3800$ and 4500 we found Floquet states with very prominent peaks near $(x=1,\ p=0)$. The Husimi distributions of these states are shown in Fig. 8. However, for $\epsilon=5000$ we were unable to find any Floquet states with a prominent peak at $(x=1,\ p=0)$. This is in agreement with what is seen in Fig. 7. The enhanced localization due to the ZC orbits appears to continue for $\epsilon>3200$, but for $\epsilon\geqslant 5000$ the effects of the ZC orbits are no longer apparent.

VI. CONCLUSION

A sinusoidally driven classical particle in an infinite square well displays predominantly chaotic motion at low momentum when the strength of the driving field is sufficiently high. Buried within the chaotic region of the phase space for this system is a continuous line of marginally stable periodic orbits which we call "zero-collision" orbits because they never collide with the walls of the well. We have shown that the quantum version of this system has Floquet eigenstates that are strongly localized in the vicinity of the ZC orbits. Surprisingly, the increased localization associated with the ZC orbits seems to persist at field strengths beyond that at which the ZC orbits themselves disappear. This may be an example of scarring by the "ghost" of a family of periodic orbits.

The ZC states are not the first examples of quantum states that are strongly localized along a line of marginally stable periodic orbits. The "bouncing ball" energy eigenstates seen in a number of billiard systems illustrate the same effect [5,6]. Similar bouncing ball states have been identified among the Floquet eigenstates of a δ-kicked system related to the Sinai billiard [17]. To our knowledge, though, the ZC states are the first example of this effect in a continuously driven system. The bouncing ball states form a set of measure zero in the semiclassical limit and thus do not contradict Schnirelman's theorem [8]. We would expect the ZC states to follow the same pattern and persist as $\hbar \to 0$, but form an ever decreasing fraction of the overall set of quantum eigenstates. We intend to explore this conjecture in future work, with particular emphasis on the ghost ZC states that exist at field strengths beyond that at which the ZC orbits are destroyed.

The bouncing ball states in billiard systems give rise to experimentally detectable effects [7]. The presence of the ZC states in our model may also be detectable in experiments involving trapping potentials with flat regions, such as an electron in a $GaAs/Al_xGa_{1-x}As$ quantum wells subject to intense far-infrared radiation [18]. This effect might be used to localize and trap low-energy electrons in the presence of radiation. Since the ZC states are localized at low energies, an electron in a ZC state will be less likely to be ejected from the well.

ACKNOWLEDGMENTS

L.E.R. wishes to thank the Robert A. Welch Foundation (Grant No. F-1051) and F.P. wishes to thank the Berry College Office of Student Work for partial support of this work.

[1] L. E. Reichl, *The Transition to Chaos: Conservative Classical Systems and Quantum Manifestations*, 2nd ed. (Springer-Verlag, New York, 2004).
[2] E. J. Heller, Phys. Rev. Lett. **53**, 1515 (1984).
[3] P. W. Anderson, Phys. Rev. **109**, 1492 (1958).
[4] R. C. Brown and R. E. Wyatt, Phys. Rev. Lett. **57**, 1 (1986).
[5] P. W. O'Connor and E. J. Heller, Phys. Rev. Lett. **61**, 2288 (1988).
[6] E. Bogomolny and C. Schmit, Phys. Rev. Lett. **92**, 244102 (2004); G. Berkolaiko, J. P. Keating, and B. Winn, *ibid.* **91**, 134103 (2003); T. Papenbrock and T. Prosen, *ibid.* **84**, 262 (2000); D. Biswas and S. R. Jain, Phys. Rev. A **42**, 3170 (1990).
[7] H. Alt, C. Dembowski, H.-D. Gräf, R. Hofferbert, H. Rehfeld, A. Richter, and C. Schmit, Phys. Rev. E **60**, 2851 (1999); S. Sridhar, Phys. Rev. Lett. **67**, 785 (1991).
[8] A. I. Schnirelman, Usp. Mat. Nauk **29**, 181 (1974); S. Zelditch, Duke Math. J. **55**, 919 (1987); Y. Colin de Verdiere, Commun. Math. Phys. **102**, 497 (1985).
[9] W. A. Lin and L. E. Reichl, Physica D **19**, 145 (1986).
[10] J. H. Shirley, Phys. Rev. **138**, B979 (1965).
[11] H. Sambe, Phys. Rev. A **7**, 2203 (1973).
[12] T. Timberlake and L. E. Reichl, Phys. Rev. A **59**, 2886 (1999).
[13] K. Husimi, Proc. Phys. Math. Soc. Jpn. **22**, 246 (1940); K. Takahashi, Prog. Theor. Phys. Suppl. **98**, 109 (1989).
[14] W. E. Bies, L. Kaplan, M. R. Haggerty, and E. J. Heller, Phys. Rev. E **63**, 066214 (2001).
[15] Y. Y. Bai, G. Hose, K. Stefański, and H. S. Taylor, Phys. Rev. A **31**, 2821 (1985).
[16] P. Bellomo and T. Uzer, Phys. Rev. E **50**, 1886 (1994).
[17] L. Kaplan and E. J. Heller, Phys. Rev. E **62**, 409 (2000).
[18] B. Birnir, B. Galdrikian, R. Grauer, and M. Sherwin, Phys. Rev. B **47**, R6795 (1993); B. Galdrikian, B. Birnir, and M. Sherwin, Phys. Lett. A **203**, 319 (1995).